



A new uniform parameterization and invariant 3D spherical harmonic shape descriptors for shape analysis of the heart's left ventricle – A pilot study

A. Ben Abdallah^{a,*}, F. Ghorbel^b, K. Chatti^a, H. Essabbah^a, M.H. Bedoui^a

^a Laboratoire de Biophysique – TIM, UR 08-27, Monastir, Tunisia

^b Laboratoire CRISTAL – Pole GRIFT, Ecole Nationale des Sciences de l'Informatique, Campus Universitaire, la Manouba, Tunisia

ARTICLE INFO

Article history:

Received 21 April 2009

Available online 25 June 2010

Communicated by F.Y. Shih

Keywords:

Spherical harmonic model

Uniform parameterization

Rotation invariant 3D shape descriptors

Left ventricle

Myocardial scintigraphy

ABSTRACT

A new approach for uniform parameterization and rotation invariant global description of 3D triangular surface meshes of objects with a spherical topology is presented. It consists of two steps. First, an initial mapping based on a heat conduction model is carried out and an optimization of the initial parameterization in a constrained optimization procedure is applied. Second, a rotation invariant 3D shape description is achieved using the abstract harmonic analysis and the shift theorem. Our approach is validated on both synthetic data and real data obtained from myocardial scintigraphy imaging technique as an example.

© 2010 Elsevier B.V. All rights reserved.

1. Introduction

3D medical imagery has witnessed great progress in the last 20 years. It has allowed a better characterization of the explored organ's shape and a better assessment of its function. Although the global vision of the organ aids diagnosis and therapy, it does not allow any deformation quantification, thereby making it necessary to ensure the 3D structures' geometrical representation in order to extract shape and motion descriptors.

Several approaches have been used for 3D anatomical structure modeling, particularly the heart, using various medical imaging techniques. For example, [Cauvin et al. \(1993\)](#) applied algebraic surfaces to model the ventricle using SPECT (Single Photon Emission Computed Tomography) images. [Bardinet et al. \(1994\)](#) used the parametric superquadric model associated to free-form deformations (FFD) to characterize the heart motion over time using tomographic images and the superquadric model tracked as a reference shape and combined with displacement function. Various approaches namely the hyperquadric one ([Han and Goldgof, 1993](#)) were used for cardiac 3D images analysis. [Kelemen et al. \(1999\)](#) applied the spherical harmonic basis functions (SPHARM) proposed by [Brecbühler et al. \(1995\)](#) to evaluate a population of 3D hippocampus shapes and demonstrated that SPHARM could be used to express shape deformations. [Styner et al. \(2004\)](#) used SPHARM

for the analysis of the hippocampus shape abnormalities in schizophrenia. [Huang et al. \(2005\)](#) proposed a surface matching technique for 3D SPHARM models based on the rotational properties of the harmonic analysis to align objects in order to determine correspondence between shapes. They applied their techniques in cardiac MRI to assess changes in the wall thickness of the left ventricle of the heart. [Glodberg-Zimring et al. \(2005\)](#) adopted the spherical harmonics to estimate the volume of brain tumors using magnetic resonance images from five patients.

Knowing that the left ventricle of the heart is a closed surface with a spherical topology, we propose the spherical harmonic basis functions to approximate its 3D shape and the abstract harmonic analysis to generate rotation invariant 3D shape descriptors.

We aim to measure and analyze the heart's left ventricle deformation at stress and rest in order to quantify the severity of the heart pathology using the scintigraphic imaging technique and the spherical harmonic basis functions.

For this purpose, we have to resolve a key problem which is the appropriate parameterization necessary for the use of spherical harmonic functions in 3D shape description. In fact, it is necessary to have a homogenous distribution of the 3D points on the surface in order to accurately generate coefficients of a series representing the 3D object. Most of the works achieved in this context have proposed solutions adapted to specific surfaces such as superquadrics ([Bardinet et al., 1994](#); [Vemuri and Radisavljevic, 1993](#)) and hyperquadrics ([Han and Goldgof, 1993](#)). [Vemuri and Radisavljevic \(1993\)](#) overcame this problem by the resolution of a differential equation. [Bardinet et al. \(1994\)](#) proposed a less expensive solution. He projected the set of points from the sphere to the ellipsoid, then from

* Corresponding author. Tel.: +216 93503139; fax: +216 73462200.

E-mail addresses: asma.babdallah@crystal.rnu.tn (A.B. Abdallah), Fauzi.Ghorbel@Ensi.rnu.tn (F. Ghorbel), habib.essabbah@topnet.tn (H. Essabbah), MedHedi.Bedoui@fmm.rnu.tn (M.H. Bedoui).

the ellipsoid to the superellipsoid to get better uniform distribution points. The resulting points are regularly spaced on the surface. The generation of such a parameterization was formulated and solved as a large constrained optimization problem by Brechbühler et al. (1995). As an input, the algorithm used a closed surface represented by square faces mesh. It overcame limitations of expressing an object surface by explicit parametric representations, which were restricted to star-shaped objects, and the non-uniform spacing of parameters on the object surface. The initial approach of Brechbühler et al. (1995) was modified by Quicken et al. (2000) who used triangulated surfaces as an input for the parameterization algorithm. To obtain a homogenous distribution of the parameter space over the surface, the initial parameterization was modified in a constrained optimization procedure exploiting the knowledge that triangles are obtained by dividing equal-sized squares. Accordingly, angles of each triangle and the side lengths are known. In (Sijbers and Van Dyck, 2002), a uniform surface parameterization was achieved by initially using an inflation algorithm to map polygonized 3D objects to a unit sphere. A homogeneous distribution of the vertices was achieved by applying an iterative watershed algorithm to the surface graph.

In this paper, we present a new technique for the uniform parameterization of 3D triangular mesh surfaces of objects with spherical topology based on works in (Brechbühler et al., 1995; Quicken et al., 2000) and rotation invariant shape description based on the abstract harmonic analysis and the shift theorem to extract rotation invariant 3D shape descriptors (Burel and Henocq, 1995; Kazhdan et al., 2003; Makadia and Daniilidis, 2003).

As an illustration of the new technique, we propose to use the spherical harmonic model and data extracted from scintigraphic images to model the left ventricle of the heart. First, we started by segmenting the original scintigraphic data and separating the anatomical structures of interest, namely the epicardium wall and the endocardium wall. Then, after surface triangulation and uniform parameterization, we fitted the surface which was decomposed into a spherical harmonic basis on this set of 3D points through an iterative reconstruction process leading to determine the optimal harmonic number. Finally, based on spherical harmonic coefficients, we extracted the invariant spherical harmonic shape descriptors which would be used to compute the distance between the different anatomical structures to detect any pathology and quantify it.

The rest of this paper is organized as follows. In Section 2 we present the new parameterization algorithm including the initial mapping to obtain starting values and the nonlinear optimization process. Section 3 explains the expansion of a 3D shape into a set of spherical harmonics. In Section 4 we present the generation of rotation invariant 3D shape descriptors based on the abstract harmonic analysis and the shift Theorem. In Section 5 we present the material used to validate our approach. In Section 6 we test our

method, using myocardial scintigraphic data of a group of 37 patients. Section 7 summaries our results and discusses the possible topics for future works.

2. Surface parameterization

A triangular surface mesh was used as an input for the parameterization process. The object surface was assumed to be closed and topologically equivalent to the sphere. First, a harmonic map was created to initially map the mesh vertices from the object space to the parameter space (unit sphere) (Fig. 1) based on a heat conduction model (Brechbühler et al., 1995). To obtain a homogenous distribution of the parameter space over the surface with minimal local distortion, we modified the initial parameterization in a constrained optimization procedure considering three criteria: Euclidian norm, area uniformity and minimal distortion.

In the following section, $n_{vertices}$ denotes the vertices number, n_{faces} the triangles number, and n_{edges} the edges number. There are $3n_{vertices}$ degrees of freedom to place $n_{vertices}$ vertices on the sphere. Imposing constraints on the Euclidian norm of any vertex which must be 1 takes $n_{vertices}$ degrees of freedom and on area preservation takes $n_{faces} - 1$ degrees of freedom because the area of all triangles equals 4π .

Using Euler's equation for planar graphs: $n_{vertices} - n_{edges} + n_{faces} = 2$ and $n_{edges} = 3n_{vertices} - 6$ for triangular mesh we get $3n_{vertices} - n_{vertices} - (n_{faces} - 1) = 2$ degrees of freedom. Three global rotational degrees of freedom remain after optimization.

Two degrees of freedom are not sufficient to minimize the distortion. We changed the constraints and objective function initially proposed by Brechbühler and Quicken as follows:

1. The Euclidian norm of the coordinate of any vertex must be 1. This constraint forces every vertex to lie on the unit sphere.
2. Area uniformity: Every object face should map onto an elementary face in the parameter space. The elementary face area is obtained by dividing 4π by the total number of faces: $4\pi/n_{faces}$. Area uniformity is achieved by summing up the squared differences of the area of the triangular facets and the elementary facet area in the parameter space.
3. Minimal distortion: Every triangle should map onto an elementary spherical triangle in the parameter space. To quantify distortion, we propose to compare directly each angle in object and parameter space.

We propose an objective function which is a linear combination of area uniformity and distortion quantification (Eq. (1)):

$$\min_f \sum_{i \in A} \left[|area_{p,i} - (4\pi/n_{faces})|^2 + \sum_{j=0}^2 |\cos \alpha_{ijp} - \cos \alpha_{ijo}|^2 \right] \quad (1)$$

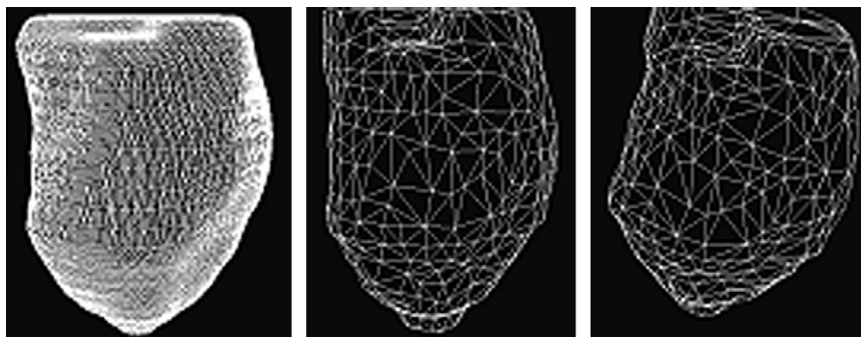


Fig. 1. Mapping of triangular faces on the object's surface (object space) to spherical triangles (parameter space).

where f is the mapping function from the object space to the unit sphere that assigns values to every vertex of the triangular mesh, $area_{p,i}$ denotes the facet area of the triangle i ($i = 1, \dots, n_{faces}$) in the parameter space, $\cos \alpha_{ijp}$ ($\cos \alpha_{ijo}$, respectively) is the angle cosinus of the triangle i in the parameter space (object space respectively) and j varies from 0 to 2.

3. Spherical harmonic descriptors

The spherical harmonic surface can be written as an expansion of spherical harmonic basis functions for the three coordinates. A set of coefficients is then used to express the surface in a compact way (Eq. (2)):

$$S(\theta, \phi) = (x(\theta, \phi), y(\theta, \phi), z(\theta, \phi))^T = \sum_{l=0}^L \sum_{m=-l}^l c_l^m Y_l^m(\theta, \phi), \quad (2)$$

where $c_l^m = (c_{xl}^m, c_{yl}^m, c_{zl}^m)^T$ are 3D vectors and they are obtained by solving a least-squares problem.

The values of the basis functions are gathered in the matrix $B = B_{ij(l,m)}$ with $B_{ij(l,m)} = Y_l^m(\theta_i, \phi_i)$ where $j(l, m)$ is a function assigning an index to every pair (l, m) and i denotes the indices of $n_{vertices}$ points to be approximated. The coordinates of these points are saved in $S = (S_1, S_2, \dots, S_{n_{vertices}})^T$ and all coefficients are stored in the matrix $C = (C_0^0, C_1^{-1}, C_1^0, \dots)^T$.

Starting values of c_l^m coefficients are given by (Eq. (3)):

$$c_l^m = 4\pi \left/ n_{vertices} \sum_{i=0}^{n_{vertices}-1} S_i(\theta_i, \phi_i) Y_l^m(\theta_i, \phi_i) \right. \quad (3)$$

The coefficients that best approximate the points in a least-squares sense are obtained by (Eq. (4)):

$$C = (B^T B)^{-1} B^T S \quad (4)$$

Using the spherical harmonic basis we obtained a hierarchical surface description which includes further details as more coefficients are considered (Fig. 2).

4. Invariant 3D shape descriptors

The properties of invariance are required to eliminate differences due to rotation, translation and magnification (Fig. 3). To get rid of these dependencies, the models are usually normalized by using the center of mass for translation, the root of the average square radius for scale and principal axes for rotation (Brecbühler et al., 1995; Gerig et al., 2001). It is well known that while translation and scale normalization methods are robust, the rotation normalization via PCA-alignment does not provide a robust normalization. To overcome this limitation, and knowing that the

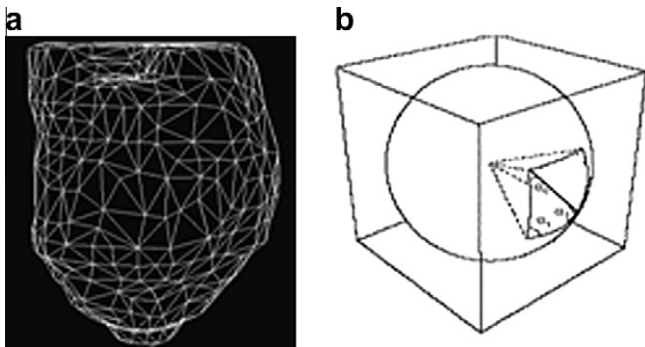


Fig. 2. Rendered surface of the object (a) (respectively (d)). Global shape description by expansion into spherical harmonics. Reconstruction up to degrees 4 (b) and 6 (c) (respectively degree 4 (e) and 5 (c)).

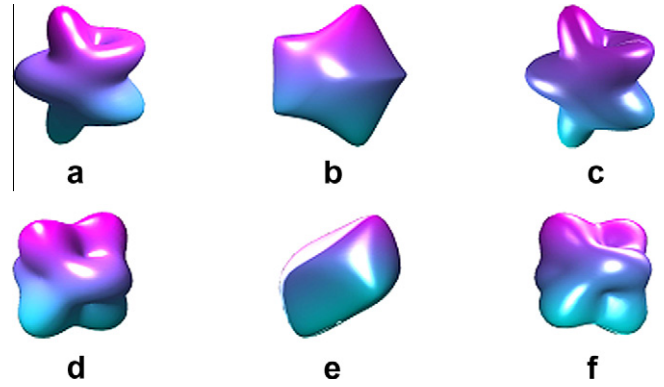


Fig. 3. Visualization of the same object described by three different point clouds. The number of vertices (a) 8128, (b) 900, (c) the point clouds described in (b) and having undergone a rotation.

heart's left ventricle has a spherical topology, we propose to use the abstract harmonic analysis and the shift theorem to extract rotation invariant 3D shape descriptors (Burel and Henocq, 1995; Kazhdan et al., 2003; Makadia and Daniilidis, 2003).

To achieve the translational invariance, we placed the origin of 3D coordinates at the center of gravity of the object. To obtain the scale invariance, we divided all the spherical harmonic coefficients by the distance between the origin and the farthest point of the object.

4.1. Spherical Fourier transform

Points on the unit sphere S^2 are parameterized using the spherical coordinates $\theta \in [0, \pi]$, $\phi \in [0, 2\pi]$. Any point $\eta(\theta, \phi) \in S^2$ is written as the unit vector $\eta(\theta, \phi) = (\cos \phi \sin \theta, \sin \phi \cos \theta, \cos \theta)$. $f(\theta, \phi)$ is denoted for any function whose domain is restricted to the unit sphere. The integration of a function $f(\theta, \phi) \in L^2(S^2)$ is defined as (Eq. (5)):

$$\int_0^\pi \int_0^{2\pi} f(\theta, \phi) d\phi \sin \theta d\theta \quad (5)$$

where $d\phi \sin \theta d\theta$ is the rotation-invariant measure on the sphere.

On the sphere, the spherical harmonics form an orthonormal basis for $L^2(S^2)$. Any function $f(\theta, \phi) \in L^2(S^2)$ can be expanded in this basis as (Eqs. (6) and (7)):

$$f(\theta, \phi) = \sum_{l=0}^L \sum_{m=-l}^l c_l^m Y_l^m(\theta, \phi) \quad (6)$$

where c_l^m denotes the harmonic coefficients,

$$c_l^m = \int_0^\pi \int_0^{2\pi} f(\theta, \phi) \bar{Y}_l^m(\theta, \phi) d\phi \sin \theta d\theta \quad (7)$$

Sphere S^2 is a homogenous space. $SO(3)$ is a compact and unimodular group which can act on sphere S^2 . The Fourier series of a group exists if the group possesses an irreducible unitary representation. From a group theory point of view, the spherical harmonics are a complete basis for the irreducible representations of the rotation group $SO(3)$. This property presents a way for decomposing spherical functions into rotation invariant components. In our case, the coefficients of the spherical Fourier transform are the expansion coefficients c_l^m of the function $f(\theta, \phi)$ in the basis of spherical harmonics.



Fig. 4. Rendered surface of O1 object.

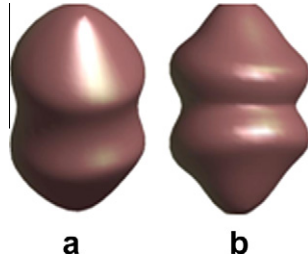


Fig. 5. Reconstruction of O1 up to degrees 4 and 10 ((a) and (b) respectively).

5. Material

In this section we present our materials. First, we describe the synthetic models used to validate the global description and extraction of the invariant 3D descriptors. Then, we provide an example of a 3D surface reconstruction using nuclear medicine

4.2. Computation of rotation invariant spherical harmonic descriptors

Knowing that a rotated spherical harmonic of degree l can be written as a linear combination of spherical harmonics of the same degree l and that spherical harmonic coefficient of a rotated $\lambda_g f(\theta, \varphi)$ function is a linear combination of the coefficients of the function $f(\theta, \varphi)$, the shift theorem allows us to define real value functions $I_l(f(\theta, \varphi))$ which remain invariant under rotations (Eq. (8)):

$$I_l(f(\theta, \varphi)) = \sum_{|m| \leq l} \bar{C}_l^m C_l^m \tag{8}$$

where C_l^m are the coefficients of $f(\theta, \varphi)$, \bar{C}_l^m denotes the conjugate complex of C_l^m and I_l the $(2l + 1) \times 1$ column vector of all coefficients of degree l , $g \in SO(3)$ and λ_g its associated operator.

4.3. Distance measure between spherical harmonic models

Rotating a spherical harmonic function does not affect its L_2 -norm. We propose to use the L_2 -difference between two spherical harmonic models f and g in order to compare and discriminate them. Based on the rotation invariant descriptors (Section 4.2), we define the following distance measure D as follows:

$$D(f, g) = \sqrt{\sum_i (I_{f,i} - I_{g,i})^2} \tag{9}$$

where $I_{f,i}$ and $I_{g,i}$ stand for i th invariant of the spherical harmonic models f and g , respectively.



Fig. 6. Rendered surface of O2 object.

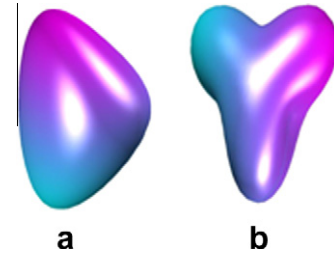


Fig. 7. Reconstruction of O2 up to degrees 3 and 4 ((a) and (b) respectively).



Fig. 8. Rendered surface of O3 object.

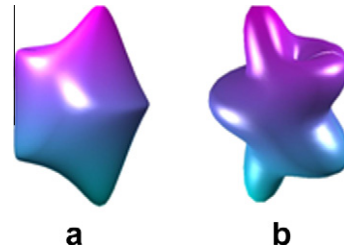


Fig. 9. Reconstruction of O3 up to degrees 4 and 6 ((a) and (b) respectively).



Fig. 10. Rendered surface of O4 object.

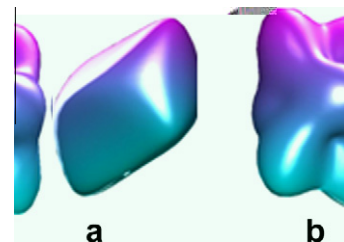


Fig. 11. Reconstruction of O4 up to degrees 4 and 6 ((a) and (b) respectively).

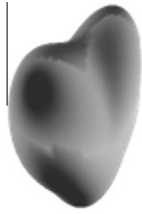


Fig. 12. Rendered surface of O5 object.

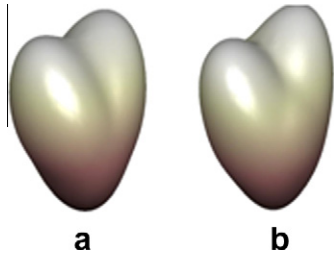


Fig. 13. Reconstruction of O5 up to degrees 4 and 6 ((a) and (b) respectively).

images in order to show our approach can numerically quantify organ deformations.

5.1. Synthetic data

Six synthetic 3D triangular mesh surfaces of objects with spherical topology were used. Five with arbitrary complexity shapes (Figs. 4, 6, 8, 10 and 12) and one was a non star-shaped object (Fig. 14).

5.2. Scintigraphic images

We used myocardium SPECT (Single Photon Emission Computed Tomography) images performed at stress and rest on 37 patients from the Nuclear Medicine Department of The University Hospital Sahloul, Sousse, Tunisia. The myocardium scintigraphy (Matsunari et al., 1997; Hambÿe et al., 2007) was performed to diagnose coronary artery disease (CAD) for each of them. This diagnosis was based on the determination of the site, the extent and the severity of the pathology on both stress and rest sequences (Fig. 18). The Myocardium SPECT results were reviewed by two qualified nuclear medicine physicians. Ten exams were declared as healthy, sixteen with moderate CAD and 11 with severe CAD.

5.2.1. Segmentation and 3D reconstruction of the heart's left ventricle

As an input, we used 2D slices of the heart's left ventricle at stress and rest. We started by segmenting the original scintigraphic

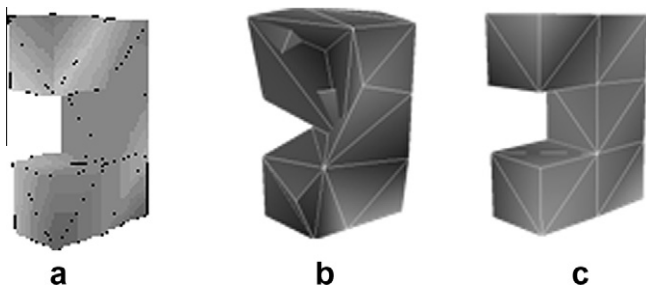


Fig. 14. (a) Rendered surface of O6 object. Reconstruction of O6 up to degrees 5 and 10 ((b) and (c) respectively).

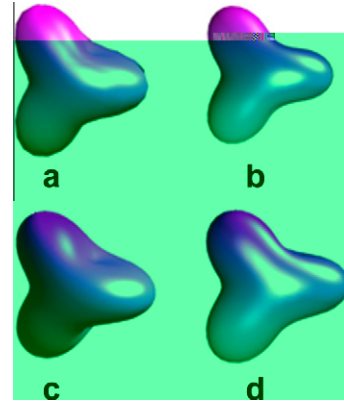


Fig. 15. (a) Rendered surface of O1 object (vertices number 121). (b) Reconstruction up to degree 4. (c) Rendered surface of O8 object (vertices number 6562). (d) Reconstruction up to degree 4.

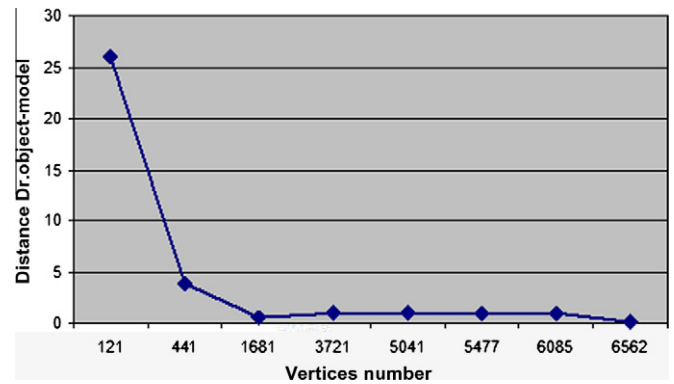


Fig. 16. The distance between the object and the model_j (with $j = 1-8$).

data and separating the anatomical structures of interest, namely the epicardium wall and the endocardium wall (Fig. 19). Fig. 20 shows an example of a rendered surface of the left ventricle at stress and rest respectively after the segmentation of scintigraphic image sequences of one patient.

5.2.2. Data base structure

For each patient we extracted four triangulated meshes representing the surface of the anatomical structures of the epicardium wall at rest (EPR), the epicardium wall at stress (EPS), the endocardium wall at rest (ENR) and the endocardium wall at stress (ENS). For each mesh, the number of triangles is 1000 and the number of vertices is 502. All the generated triangulated meshes would be used as the input for the 3D spherical harmonic shape description process (Figs. 21 and 22). Table 1 sums up the expert's diagnosis for each patient.

6. Results

6.1. Synthetic data

First, we present the results of a global description for each object. Then we test the influence of the variation of the triangular mesh as an input on the capacity of the model to represent correctly the original object. Finally we verify the translation, scale and rotation invariance of our shape descriptors.

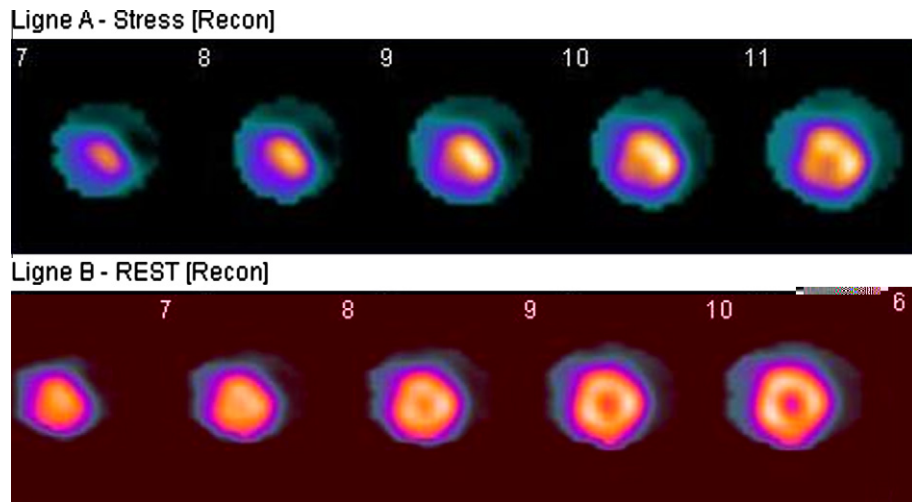


Fig. 17. Rotation of the O4 object around z-axis.

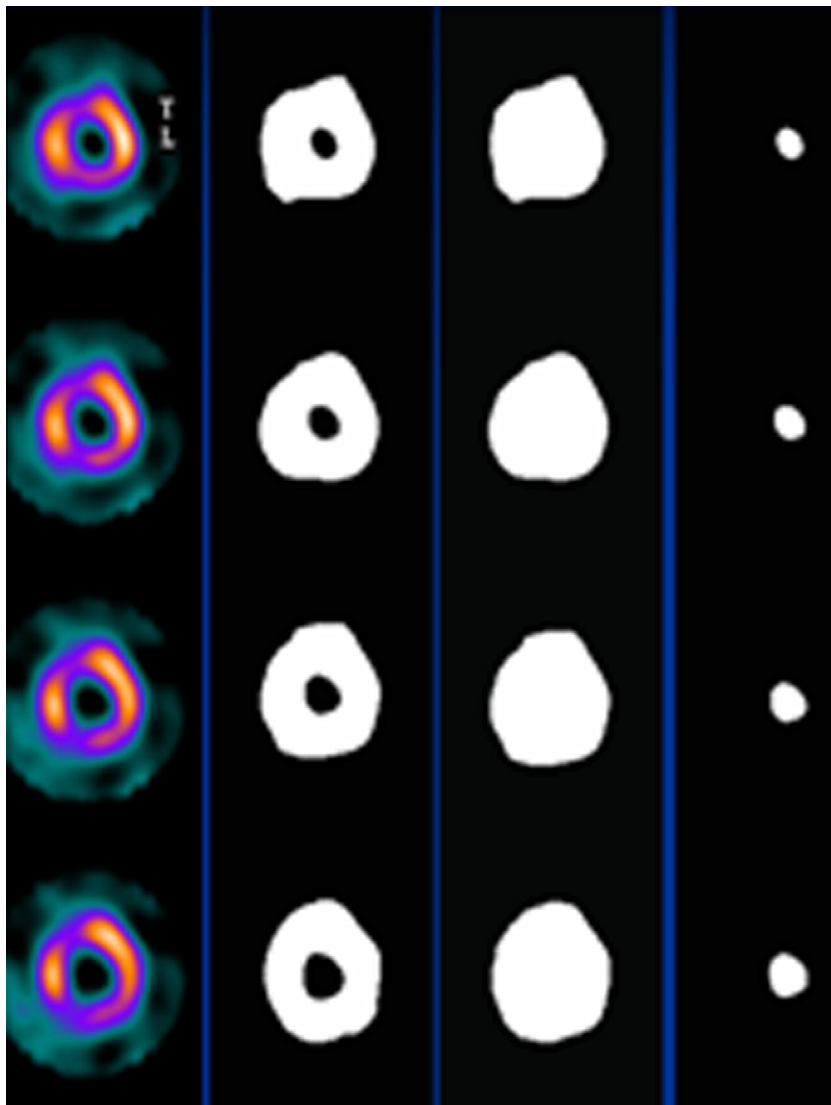


Fig. 18. Scintigraphic image sequences at stress and rest for one patient.

6.1.1. Global description by expansion into spherical harmonics

The triangulated surfaces of the test objects were parameterized as described in Section 2, and their shapes were expressed through spherical harmonic descriptors as described in Section 3.

Fig. 4 (Figs. 6, 8, 10, 12 and 14, respectively) shows an example of a synthetic 3D object rendered surface. Fig. 5 (Figs. 7, 9, 11, 13 and 15, respectively) shows the reconstruction of the surface object with the spherical harmonic model using (Eq. (6)).

The surface parameterization technique is no longer restricted to star-shaped or convex objects but can be applied on arbitrarily shaped objects with a spherical topology (Fig. 14). The surface is explicitly represented by the variation of two parameters and the size of the set of coefficients can be chosen so that the spherical harmonics characterize the desired details of the shape.

6.1.2. Robustness of the spherical harmonic shape representation with respect to the input mesh

In order to test the influence of the input mesh on the global shape description by the spherical harmonic approach, we used

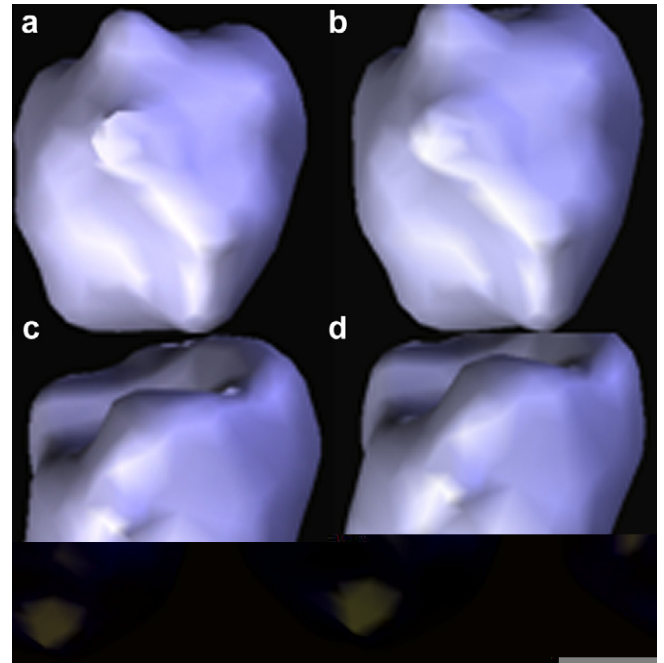


Fig. 21. Left to right (a) rendered surface of the epicardium wall in patient 1. (b) Epicardium modeling with SH model at stress. Reconstruction up to degree 10. (c) Rendered surface of the epicardium wall in patient 1. (d) Epicardium modeling with SH model at rest. Reconstruction up to degree 10.

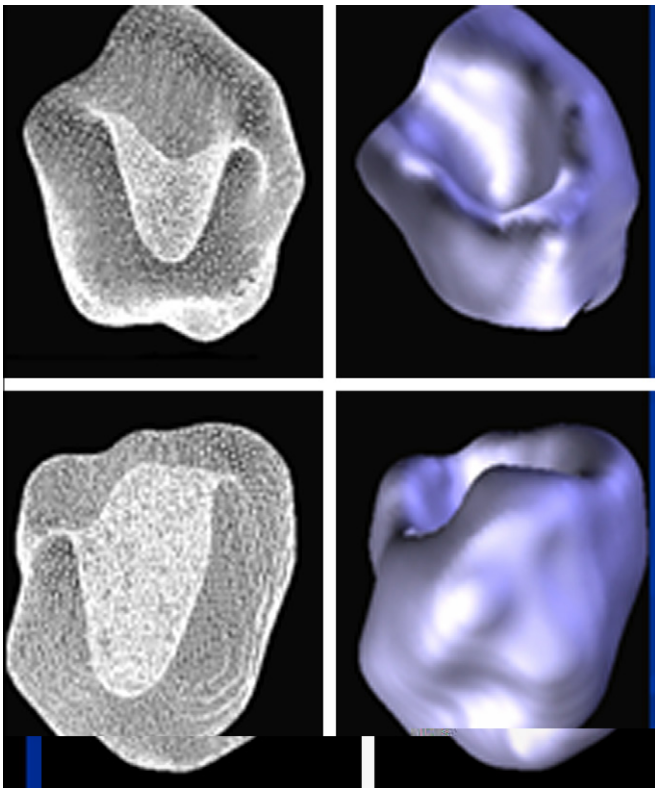


Fig. 19. Segmentation and separation of scintigraphic image sequences in one patient resulting in the structures of the epicardium wall and the endocardium wall.

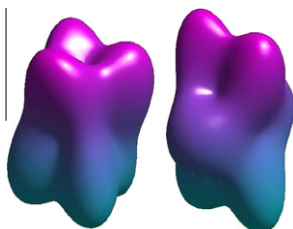


Fig. 20. Rendered surface of the left ventricle at stress and rest respectively after segmentation of scintigraphic image sequences in one patient.

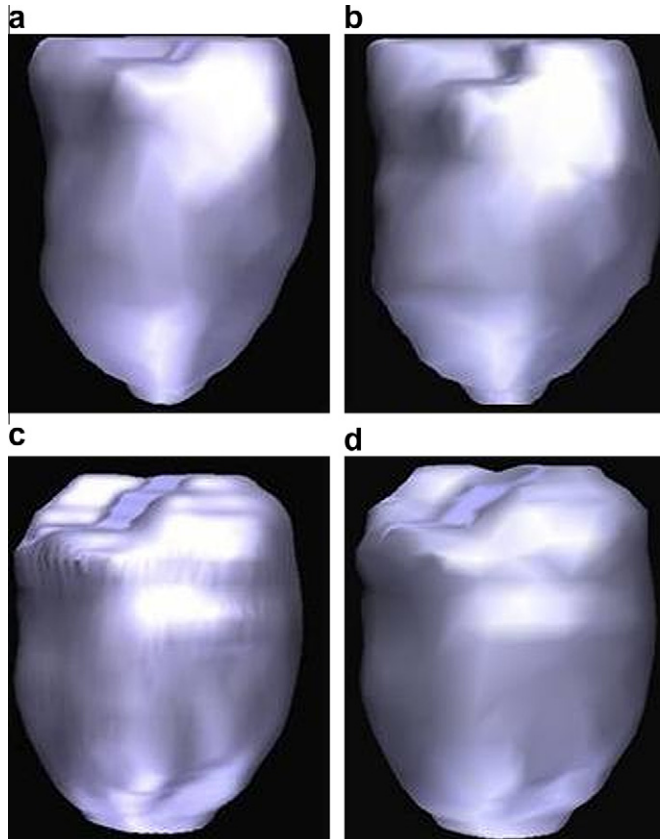


Fig. 22. Left to right (a) rendered surface of the epicardium wall of patient 1. (b) Epicardium modeling with SH model at stress. Reconstruction up to degree 10. (c) Rendered surface of the epicardium wall of patient 1. (d) Epicardium modeling with SH model at rest. Reconstruction up to degree 10.

Table 1
Expert diagnosis for the 37 patients.

Patient	Diagnosis
1	Healthy
2	Critical
3	Moderate
4	Moderate
5	Critical
6	Moderate
7	Critical
8	Critical
9	Critical
10	Moderate
11	Moderate
12	Moderate
13	Critical
14	healthy
15	healthy
16	healthy
17	critical
18	Moderate
19	Critical
20	Moderate
21	Moderate
22	Healthy
23	Healthy
24	Critical
25	Moderate
26	Critical
27	Moderate
28	Critical
29	Moderate
30	Moderate
31	Healthy
32	Moderate
33	Moderate
34	Moderate
35	Healthy
36	Healthy
37	Healthy

Table 3

(a) Comparison of epicardium wall invariant distance at stress and at rest. (b) Comparison of endocardium wall invariant distance at stress and at rest for 37 patients.

Patient number	Distance between epicardium wall and endocardium wall at stress using invariant SH shape descriptors (a)	Distance between endocardium wall at stress and at rest using invariant SH shape descriptors (b)
1	0.119	0.025
2	0.054	0.050
3	0.124	0.05
4	0.2	0.11
5	0.051	0.030
6	0.112	0.064
7	0.062	0.082
8	0.122	0.167
9	0.030	0.034
10	0.080	0.088
11	0.063	0.017
12	0.082	0.154
13	0.058	0.11
14	0.184	0.09
15	0.128	0.068
16	0.083	0.025
17	0.038	0.027
18	0.064	0.067
19	0.15	0.124
20	0.109	0.226
21	0.058	0.056
22	0.186	0.046
23	0.311	0.352
24	0.120	0.089
25	0.069	0.141
26	0.164	0.131
27	0.234	0.108
28	0.057	0.112
29	0.135	0.081
30	0.247	0.079
31	0.239	0.292
32	0.123	0.077
33	0.041	0.094
34	0.059	0.349
35	0.499	0.317
36	0.299	0.322
37	0.4275	0.181

O2 object of Fig. 6 and we generated eight different triangular meshes. The number of data points varies from 122 to 6586 and that of triangles from 238 to 13,120 (Table 2). We computed the shape descriptors of each mesh j ($j: 1, \dots, 8$) as described in Sections 2 and 3. Then we calculated the root mean squared distance (Dr_j) between the mesh j used as an input and the model j as follows (Eq. (10)):

$$Dr_j = 1 / \sqrt{n_{j\text{vertices}}} \sqrt{\sum_{i=1}^{i=n_{j\text{vertices}}} |R_{i\text{Object}_j} - R_{i\text{Model}_j}|^2} \quad (10)$$

where $R_{i\text{Object}_j}$ (respectively $R_{i\text{Model}_j}$) stands for the distance separating the vertex i of the mesh j used as an input (respectively the vertex i of the spherical harmonic model j) from the origin and $n_{j\text{vertices}}$ denotes the number of vertices of the mesh j (respectively the spherical harmonic model j) used as an input.

Table 2 sums up the average distances between the eight original objects and their models. Fig. 15(a) and (c) shows the rendered surface of the O2 object represented by meshes with 121 and 6562 vertices, respectively. Fig. 15(b) and (d) illustrates the reconstruction of the original O2 object using as an input mesh 1 and mesh 8 up to degree 4, respectively. Although there are a few data points, the original object is correctly reconstructed. It can be concluded

that the spherical harmonic global description is robust (Table 1, Fig. 16).

6.1.3. Robustness of the 3D invariance

In this section we present the results obtained using the invariant 3D shape descriptors to test their robustness with respect to translation, scale and rotation. For this purpose, we translated, scaled and rotated (Fig. 17), the synthetic O4 object (Fig. 10). We modeled the transformed objects and extracted their invariant descriptors. We computed the distance (Eq. (9)) between the original and the translated object (respectively scaled and rotated). The results demonstrated that the shape descriptors were robust with respect to translation, scale and rotation.

6.2. Shape analysis of the left ventricle of the heart

This section is devoted to real data analysis. We present the shape analysis of the heart's left ventricle (LV) in 37 patients at

Table 2
Estimated distance (Dr_j) between the original object ($j: 1, \dots, 8$) and the reconstruction up to degree 4.

Synthetic object	Mesh 1	Mesh 2	Mesh 3	Mesh 4	Mesh 5	Mesh 6	Mesh 7	Mesh 8
Vertices number	121	441	1681	3721	5041	5477	6085	6562
Dr_j distance	$26 \cdot 10^{-4}$	$3.98 \cdot 10^{-4}$	$0.569 \cdot 10^{-4}$	$1.0 \cdot 10^{-4}$	$1.0 \cdot 10^{-4}$	$1.0 \cdot 10^{-4}$	$0.996 \cdot 10^{-4}$	$0.169 \cdot 10^{-4}$

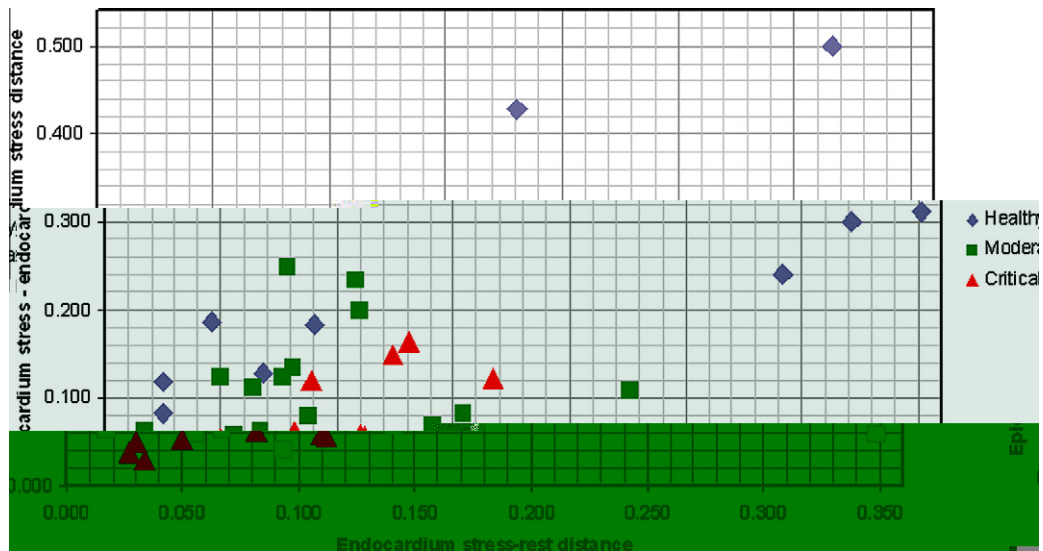


Fig. 23. Endocardium wall invariant distance (stress–rest) in terms of epicardium wall invariant distance at stress–endocardium wall invariant distance at rest).

stress and rest respectively using spherical harmonic functions and scintigraphic images (Fig. 18).

6.2.1. Global shape description and deformation quantification of the heart's left ventricle

The triangulated surfaces of these anatomical structures (Fig. 20.) were parameterized. Their shapes were expressed through spherical harmonic coefficients and their invariant spherical harmonic descriptors were extracted as described in Sections 2–4.

For the two examples (Figs. 21 and 22), we analyzed the scintigraphic data of one healthy patient and one pathological case respectively. Fig. 21 shows an example of the rendered surface of the epicardium wall at stress and rest respectively for one healthy patient (Fig. 21(a) and (c)) and epicardium modeling with SH model at stress and rest, respectively (Fig. 21(b) and (d)).

Fig. 22 shows an example of the rendered surface of the epicardium wall at stress and rest respectively for one patient (Fig. 22(a) and (c)), epicardium modeling with SH model at stress and rest, respectively (Fig. 22(b) and (d)).

6.2.2. Deformation quantification of the heart's left ventricle

Nowadays, the most common evaluation technique of the myocardium disease extent and severity in a CAD patient is a quantitative evaluation that gives the summed stress score (SSS), the summed rest score (SRS) and the summed differences score (SDS = SSS – SRS). This technique allows the evaluation of perfusion but does not take into account wall motion which is an important parameter in myocardium viability assessment.

The present approach proposes a quantitative analysis of motion based on numerical distances obtained from invariant spherical harmonic descriptors. Eq. (9) is used to compute two distances D1 and D2. D1 refers to the distance between the epicardium wall and the endocardium wall at stress (Table 3a). D2 is the distance between the endocardium wall at rest and that at stress (Table 3b). It is expected that healthy subjects are those whose D1 and D2 are high, critically-affected CAD patients have low D1 and D2 and moderately-affected patients have intermediate D1 and D2 values. The curve D1 in function of D2 is plotted to check this expected classification (Fig. 23).

Most patients were well-plotted on the curve. Some healthy patients were closer to moderate ones and some moderate patients

were closer to critically affected ones. These ambiguities could be due to:

- segmentation and closed contour approach which is manipulator-dependent and improves with expertise and experience,
- dynamic stress or pharmacological stress test,
- patient's gender,
- clinical data (diabetes, hypertension, ...).

7. Conclusion

In this work, we presented a new technique to generate triangular mesh surface parameterization and characterize 3D surfaces by invariant spherical harmonic shape descriptors. First, an initial continuous mapping was achieved in spherical coordinates based on a heat conduction model as described in (Brecbühler et al., 1995; Quicken et al., 2000). Then, the initial parameterization was modified in a constrained optimization procedure to obtain a homogenous distribution of the vertices on the unit sphere surface. The parameterization controlled by the geometry of the original shape minimized local distortions and area uniformity.

The new algorithm we developed enabled us to parameterize 3D triangular mesh surfaces of objects with a spherical topology into a series of spherical harmonic functions. This global description proved effective even for surfaces represented by a reduced number of points.

Since we were interested in measuring and analyzing object deformation, the invariance of the spherical harmonic descriptor set was accomplished to eliminate differences due to rotation, translation and magnification. The translation invariance was performed by placing the origin of 3D coordinates at the center of gravity of the object. The scale invariance was achieved by choosing the distance between the origin and the farthest point of the object as unit of length. Finally, based on the harmonic analysis and applying results from the representation theory, we extracted rotation invariant 3D spherical harmonic descriptors using the shift theorem.

The invariant shape descriptors obtained were tested on synthetic 3D objects with a spherical topology. The robustness of our method to characterize and analyze the shape with respect to standard transformations allowed us to apply this approach using medical data from myocardium SPECT. The 3D invariant descriptors were used to analyze and quantify the left ventricle

model deformation at stress and rest. The two most relevant calculated numerical distances were D1 and D2. D1 refers to the distance between the epicardium wall and the endocardium wall at stress and D2 is the distance between the endocardium wall at rest and that at stress.

Using D1 and D2 parameters, the classification of most patients complied with our expected values, i.e. D1 and D2 are high for healthy subjects, low in critically-affected CAD patients and intermediate in moderately-affected ones.

This comparison between patients has been made possible by our shape descriptors being rotation, translation and scale invariant. Nevertheless, the real clinical evidence can be provided only if we use a great sample population of healthy subjects (having no hypertension, diabetes, rest electrogram abnormalities or any known heart diseases) in order to determine the range of normal values of the used parameters. This is an entirely ongoing clinical exploration.

For better results and a clear-cut distinction between subjects, our patient data basis needs to be improved and divided into sub-classes according to gender and risk factors (diabetes, hypertension, . . .). Furthermore, progress towards a regional analysis of deformations should be made to better qualify and quantify the disease extent.

The present procedure may prove particularly effective in quantifying the disease progression in the same patient from one examination to another and checking the outcome of the intervention (stent placement, coronary artery bypass graft).

To conclude, our approach can be used in the characterization and shape analysis of any object with a spherical topology and a closed surface, especially organ data obtained from various medical imaging techniques.

References

- Bardinet, E., Ayache, N., Cohen, L., 1994. Fitting of iso-surfaces using superquadrics and free-form deformations. In: Proc. IEEE Workshop on Biomedical Image Analysis.
- Brečbühler, Ch., Gerig, G., Kuhler, O., 1995. Parametrization of closed surfaces for 3D shape description. *Computer Image and Vision Understanding* 61 (2), 154–170.
- Burel, G., Henocq, H., 1995. Determination of orientation of 3D objects using spherical harmonics. *Graph. Model Image Process.* 57 (5), 400–408.
- Cauvin, J.C., Boire, J.Y., Zanca, M., Bonny, J.M., Maublant, J., Veyre, A., 1993. 3D modelling in myocardial 201Tl SPECT. *Comput. Med. Imaging Graph.* 17 (4–5), 345–350.
- Gerig, G., Styner, M., Jones, D., Weinberger, D., Lieberman, J., 2001. Shape analysis of brain ventricles using spharm. In: MMBIA, pp. 171–178.
- Glodberg-Zimring, D., Talos, I., Bhagwat, J., Haker, S., Black, P., Zou, K.H., 2005. Statistical validation of brain tumor shape approximation via spherical harmonics for image-guided neurosurgery. *Acad. Radiol.* 12 (4), 459–466.
- Hamblye, A.S., Delsarte, P., Vervaeke, A.M., 2007. Influence of the different biokinetics of sestamibi and tetrofosmin on the interpretation of myocardial perfusion imaging in daily practice. *Nucl. Med. Commun.* 28 (5), 383–390.
- Han, K.B.S., Goldof, D.B., 1993. Using hyperquadrics for shape recovery from range data. In: Proc. 4th ICCV, pp. 492–496.
- Huang, H., Shen, L., Zhang, R., Makedon, F., Hettelman, B., Pearlman, J., 2005. Surface alignment of 3D spherical harmonic models: Application to cardiac MRI analysis. *Med. Image Comput. Comput-Assisted Intervention* 8 (1), 67–74.
- Kazhdan, M., Funkhouser, T., Rusinkiewicz, S., 2003. Rotation invariant spherical harmonic representation of 3D shape descriptors. In: Proc. 2003 Eurographics/ACM SIGGRAPH Symposium on Geometry Processing, pp. 156–164.
- Kelemen, A., Székely, G., Gerig, G., 1999. Elastic model-based segmentation of 3D neuroradiological data sets. *IEEE Trans. Med. Imaging* 18 (10), 828–839.
- Makadia, A., Daniilidis, K., 2003. Direct 3D-rotation estimation from spherical images via a generalized shift theorem. In: Proc. IEEE CVPR, pp. 217–224.
- Matsunari, I., Fujino, S., Taki, J., Senma, J., Aoyama, T., Wakasugi, T., Hirai, J., Saga, T., Yamamoto, S., Tonami, N., 1997. Quantitative rest technetium-99m tetrofosmin imaging in predicting functional recovery after revascularization: comparison with rest-redistribution thallium-201. *J. Am. Coll. Cardiol.* 29 (6), 1226–1233.
- Quicken, A.M., Brechbühler, C., Hug, J., Blattmann, G., Székely, G., 2000. Parameterization of closed surfaces for parametric surface description. In: *Computer Vision and Pattern Recognition – (CVPR)*, pp. 354–360.
- Sijbers, J., Van Dyck, D., 2002. Efficient algorithm for the computation of 3D Fourier descriptors. In: Proc. First Internat. Symp. 3D Data Processing, Visualization, and Transmission, pp. 640–643.
- Styner, M., Lieberman, A.J., Pantazis, D., Gerig, G., 2004. Boundary and medial shape analysis of the hippocampus in schizophrenia. *Med. Imaging Anal. (MEDIA)* 8 (3), 197–203.
- Vemuri, B.C., Radisavljevic, A., 1993. From global to local, a continuum of shape models with fractal priors. In: Proc. IEEE Conf. on Computer Vision and Pattern Recognition (CVPR), pp. 307–313.